



HAL
open science

Ligand exchange reactions on chiral Au₃₈ cluster: CD modulation caused by the modification of ligand shell composition

Ani Baghdasaryan, Kevin Martin, Latevi Max Lawson Daku, Maurizio Mastropasqua Talamo, Narcis Avarvari, Thomas Bürgi

► To cite this version:

Ani Baghdasaryan, Kevin Martin, Latevi Max Lawson Daku, Maurizio Mastropasqua Talamo, Narcis Avarvari, et al.. Ligand exchange reactions on chiral Au₃₈ cluster: CD modulation caused by the modification of ligand shell composition. *Nanoscale*, 2020, pp.1-11. 10.1039/D0NR03824E . hal-02913403

HAL Id: hal-02913403

<https://univ-angers.hal.science/hal-02913403>

Submitted on 30 Nov 2020

HAL is a multi-disciplinary open access archive for the deposit and dissemination of scientific research documents, whether they are published or not. The documents may come from teaching and research institutions in France or abroad, or from public or private research centers.

L'archive ouverte pluridisciplinaire **HAL**, est destinée au dépôt et à la diffusion de documents scientifiques de niveau recherche, publiés ou non, émanant des établissements d'enseignement et de recherche français ou étrangers, des laboratoires publics ou privés.



Distributed under a Creative Commons Attribution - NonCommercial 4.0 International License

Ligand exchange reactions on chiral Au₃₈ cluster: CD modulation caused by the modification of ligand shell composition

Ani Baghdasaryan,^a Kévin Martin,^b Latévi Max Lawson Daku,^a Maurizio Mastropasqua Talamo,^b Narcis Avarvari^b and Thomas Bürgi*^a

Received 00th January 20xx,
Accepted 00th January 20xx

DOI: 10.1039/x0xx00000x

Ligand exchange reactions have become a highly versatile post-synthetic strategy to accurately engineer the ligand shell of atomically precise noble metal nanoclusters. By modifying the chemical structure of the exchanging ligand with chromophore substituents or adding chiral centers allows direct functionalization of the cluster with desired properties. As such, post-functionalized gold nanoclusters with unique physical-chemical properties found applications in optoelectronics, catalysis and biomedicine. Herein, we successfully performed ligand exchange reactions with chiral Au₃₈(2-PET)₂₄ cluster (both racemic and enantiopure forms) and helically chiral but configurationally labile 2-thio[4]helicene ligand (TH4). The reaction products with a composition of Au₃₈(2-PET)_{24-x}(TH4)_x were analyzed using UV-vis spectroscopy and MALDI mass spectrometry. It was found that up to ten 2-PET ligands can be replaced with the helicene ligand on the cluster surface according to MALDI analysis. Consequently, the UV-vis and CD spectra of the cluster have been strongly affected by the ligand exchange reaction. The intensity of CD signals of Au₃₈(2-PET)_{24-x}(TH4)_x were drastically reduced and red shifted with respect to reference Au₃₈(2-PET)₂₄ cluster. Moreover, the appearance of the other enantiomer in the HPLC chromatogram revealed the partial racemization of the cluster. Performed DFT calculations support the experimental observations and show that the observed chiroptical changes in UV-vis and CD spectra are exchange-site dependent. The calculations also demonstrate that there are charge transfer (CT) transitions between the Au₃₈ cluster and the helicene ligand. Thus the ligand is directly involved in the transitions and contributes to the electronic states comprising those transitions.

Introduction

Recently, ultra-small thiolate-protected gold nanoclusters of the formula of Au_m(SR)_n (< 2 nm core diameter) have gained tremendous interest in research due to their unique size-dependent chiroptical properties.^{1,2} Due to the nano-size regime, the distinctive quantum confinement effects result in discrete electronic energy band gap structure and molecular-like properties, such as HOMO-LUMO electronic transition, enhanced photoluminescence and intrinsic magnetism.^{3,4} These unique properties are drastically different from their larger counterparts (nanoparticles) and provide opportunities for developing new applications.^{5–10} Thus, a detailed characterization of size-dependent electronic properties such as optical absorption spectra,¹¹ circular dichroism (ECD and VCD),^{12–15} nonlinear optical properties^{16,17} and photoluminescence,^{18,19} is a prerequisite to further assess their applications. Among several clusters that have been successfully synthesized and characterized with various

physical-chemical methods,^{20,21} the atomically precise Au₃₈(SR)₂₄ cluster attracted much interest due to its intrinsic metal-based chiral features in a large optical window. Briefly, the structure of an Au₃₈ cluster consists of an Au₂₃ kernel, which is formed by the fusion of two icosahedral Au₁₃ cores having a common Au₃ face.²² Moreover, the Au₂₃ core is surrounded by three monomeric (Au-S-Au) and six dimeric (Au-S-Au-S-Au) staples. More importantly, the long staples are organized in a chiral fashion, thus giving rise to strong chiroptical responses.

Although atomically precise gold nanoclusters afford pronounced chiroptical properties, high stability and catalytic activity, the latter can further be altered by applying post-synthetic functionalization strategies: metal doping and ligand exchange.²³ Among this, ligand exchange reactions are especially useful for modifying the protective ligand shell and surface composition in a controlled manner.²³ The choice of the exchanging ligand plays a crucial role for the chiroptical properties, stability and solubility of the resulting reaction products. Furthermore, it can lead to dramatic changes of clusters' native properties. In this context, structural distortions upon attaching a new ligand to the cluster surface are highly plausible and even the transformation of clusters have been observed.^{24,25} Several examples of the ligand exchange reactions between Au₃₈ cluster and chiral 1,1'-

^a Department of Physical Chemistry, University of Geneva, 30 Quai Ernest-Ansermet, 1211 Geneva 4, Switzerland.

^b MOLTECH-Anjou, UMR 6200, CNRS, UNIV Angers, 2 bd Lavoisier, 49045 ANGERS Cedex, France

Electronic Supplementary Information (ESI) available: Synthesis procedure of TH4, experimental and calculated absorption and CD spectra, mass spectra and calculated features of selected electronic transitions. See DOI: 10.1039/x0xx00000x

binaphthyl-2,2'-dithiol (BINAS),²⁶ [2,2] paracyclophane-4-thiol (PCP-4-SH)²⁷ and achiral thiophenol²⁸ ligands have already been reported. Herein, the reactions led to obvious changes in the UV-vis spectrum associated with the formation of various species. In addition, the modification of the ligand shell composition sometimes induced instability and initiated the decomposition of the cluster in solution. However, recent studies showed that, depending on the structure of the incoming ligand, the ligand exchange reaction is not only limited to structural and geometrical distortions leading to the formation of mixed ligand shell species in solution, but also causes substantial core-size transformations and thus resulting in the appearance of different clusters in the solution.²⁹ For example, a novel Au₃₆ cluster with an unusual fcc-core structure has been synthesized as a result of a harsh etching process in the presence of a new thiol ligand.^{24,25,30}

Based on the above-mentioned works, we aimed to study the ligand exchange reaction between chiral, but conformationally labile 2-thio[4]helicene ligand and Au₃₈(2-PET)₂₄ cluster. The choice and the interest in helicenes are justified by several reasons.

First, helicenes are polycyclic aromatic compounds which present a screw-type shape and are analogues to biologically relevant compounds.³¹ Second, as helical structures, they are intrinsically chiral and possess strong chiroptical properties. The properties and the structures can be tuned by modifying its backbone, attaching functional groups or increasing the number of fused aromatic rings in the structure. The separation of *M* and *P* enantiomers of higher helicenes (starting from five membered rings if they are not substituted in position 1, see Fig. S1[†]) has already been achieved and they possess mirror images of their corresponding electronic CD spectra (ECD).³² However, unlike the higher homologues, the enantiomeric separation of [4]helicene is not possible in solution due to the low racemization barrier (<16 kJ/mol)^{33–35} and only the calculated CD spectrum is available.³²

Thus, initially, our keen interest was to examine (i) whether the attachment of the 2-thio[4]helicene ligand to the intrinsically chiral and enantiopure cluster would stabilize the chiral configuration of the ligand and whether one configuration would be preferred over the other depending on the cluster's absolute configuration and (ii) whether we would observe changes in the UV-vis spectra and enhancement of chiral signals in CD spectra upon incorporation of a chiral yet racemic ligand? This paper is aimed to answering the addressed questions based on extensive experimental and theoretical data.

Experimental Section

Materials

Hydrogen tetrachloroaurate (III) trihydrate (ACS, Alfa Aesar, 99.99%), *L*-glutathione reduced (Carl Roth AG, ≥98%), sodium borohydride (Aldrich, ≥96%) acetone (Fisher, 99.7%), toluene (Fisher, 99.9%), ethanol (Sigma-Aldrich, >99.8%), methanol (Fisher, 99.9%), 2-phenylethanethiol (Sigma-Aldrich-Fluka, 99+%), dichloromethane (Merck, 99.7+%), nanopure water

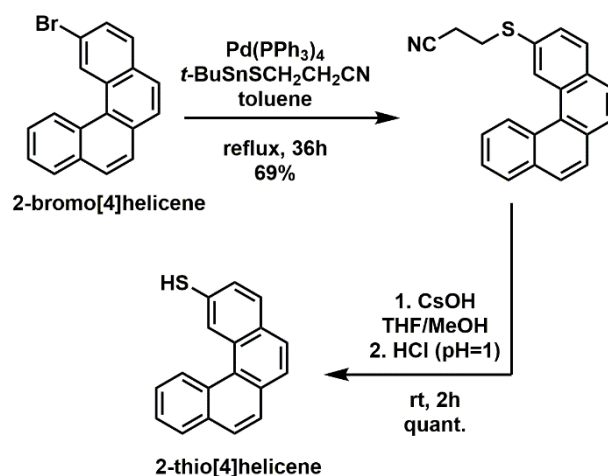
(>18 MΩ-cm), 2-thio[4]helicene ligand (TH4 shortly), 2-thio-2'-bromo[6]helicene ligand (TH6-Br shortly).

Synthesis of chiral Au₃₈(2-PET)₂₄ cluster and ligand exchange reaction with TH4 and TH6-Br ligands

Au₃₈(2-PET)₂₄ cluster was synthesized according to the previously established protocol.³⁶ Briefly, 1 g of tetrachloroauric acid trihydrate (HAuCl₄·3H₂O) dissolved in 50 mL acetone was mixed with 3.12 g *L*-glutathione (GSH) suspension in acetone and vigorously stirred for 30 min in an ice bath. Afterwards, freshly prepared and ice-cooled solution of sodium borohydride (960 mg NaBH₄ in 30 mL H₂O) was added all at once. Immediately, the reaction mixture changed its colour to dark brown corresponding to the formation of Au_m(GS)_n precipitate. The reaction mixture was left to stir at room temperature for 20 min. After that, the acetone was decanted, and the crude mixture was washed with methanol several times. Next, the GSH-protected clusters were dissolved in 30 mL of water. 1.6 mL of ethanol as a phase transfer agent together with 10 mL of toluene were also added. Then, 10 mL of 2-phenylethylthiol (2-PET shortly) ligand was added and the crude mixture was left for etching at 80 °C for 4 h. After reaction, the black precipitant was filtrated through PTFE syringe filter (0.2 μm), extensively washed with methanol to remove excess thiol and other by-products and finally dried in vacuum rotary evaporator at room temperature.

Note that the above described synthesis leads to the formation of polydisperse mixture of various particles and clusters. The separation of Au₃₈ clusters was completed with size-exclusion chromatography (SEC) using BioBeads SX-1 suspended in toluene.

The synthesis of the TH4 ligand was performed in a two-step procedure starting from 2-bromo[4]helicene^{37,38} involving first a Stille coupling reaction to introduce the propionitrile protected thiol,³⁹ and then deprotection in basic conditions and acidification (Scheme 1). The detailed description of the synthesis and the reaction conditions are given in the Supporting Information.



Scheme 1 Schematic representation of a two-step synthetic procedure for the preparation of 2-thio[4]helicene (TH4) ligand.

The synthesis of TH6-Br was performed analogously to that of TH4 starting from 2,2'-dibromo[6]helicene (see details in the Supporting Information).

Ligand exchange reaction between chiral $\text{Au}_{38}(\text{2-PET})_{24}$ cluster and TH4 ligand was carried out under mild reactions conditions (1:20, 1:50 and 1:100 cluster/ligand molar ratios, room temperature or at 50 °C, toluene solution, 24 h).

The number of exchanged ligands on the cluster surface was controlled by altering the cluster/ligand molar ratios as well as heating the solution up to 50 °C.

Ligand exchange reactions of chiral $\text{Au}_{38}(\text{2-PET})_{24}$ (racemic and enantiopure) cluster with TH6-Br ligand (racemic and enantiopure) were performed using 1:20 cluster/ligand ratios at room temperature. For enantiospecific recognition studies, the exchange reaction of racemic cluster and *M*-TH6-Br was followed *in situ* by HPLC monitoring.

Characterization methods

UV-vis spectra were recorded on the Varian Cary 50 spectrophotometer, using a quartz cuvette of 1 cm path length. Spectra were measured in toluene and normalized at 400 nm.

CD spectra were recorded on a JASCO J-815 CD-spectrometer using a quartz cuvette of 2 mm path length. The spectra were recorded in diluted solutions of DCM and the signal of the solvent was subtracted. For each spectrum, three scans at a scanning speed of 100 nm/min at a data pitch of 0.1 nm were averaged. The spectra were recorded at 20 °C; for temperature control, a JASCO PFD-350S Peltier element was used. Anisotropy factors ($\Delta A/A$) $g = \theta$ [mdeg]/(32980 × A) were calculated using the ultraviolet-visible spectrum provided by the CD spectrometer.

MALDI-TOF mass spectra were obtained using a Bruker Autoflex mass spectrometer equipped with a nitrogen laser in positive linear mode. [3-(4-tert-butylphenyl)-2-methyl-2-propenylidene]-malononitrile (abbreviated DCTB) was used as the matrix with a 1:1000 analyte : matrix ratio. 2 μl of the analyte/matrix mixture was drop cast on a plate and air-dried. Chromatographic HPLC separation of the chiral $\text{Au}_{38}(\text{2-PET})_{24}$ and exchange samples were successfully achieved on a JASCO 20XX HPLC system equipped with a semi-preparative Phenomenex Lux-Cellulose-1 column (5 μm , 250 mm × 10 mm) using n-hexane : isopropanol (80:20) mobile phase at the flow rate of 3 mL/min. The analytes were detected with a JASCO 2077 plus UV detector operated at 300 nm.

Computational methods

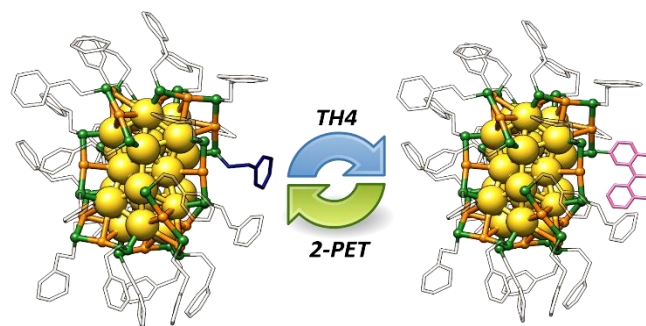
Density functional theory (DFT)^{40,41} has been applied to the optimization of the geometries of the Au_{38} clusters: the optimizations have been performed with the ADF program package (ADF2017.113 release),^{42–44} using the dispersion-corrected PBE-D3 functional^{45,46} combined with Slater-type (STO) basis set from the ADF basis set database.⁴⁷ The Au and H atoms were thus described with DZ basis sets of double-zeta quality and the other atoms by the DZP basis set of double-zeta polarized quality. The atomic core levels were kept frozen up to the 4f level for the Au atoms, and up to the 1s level for

the S and C atoms. The calculations were run spin-restricted and scalar relativistic (SR) effects were included within the zero-order regular approximation (ZORA).^{48,49}

The low-energy parts of the absorption and CD spectra of the $[\text{Au}_{38}(\text{SCH}_3)_{24}]$ model cluster have been characterized by computing with the PBE functional: the energies, oscillator and rotatory strengths of its 300 lowest-lying dipole-allowed electronic excitations within linear response theory in time-dependent DFT (TDDFT) as implemented in ADF.^{50–53} The same electronic excitation calculations were also conducted within the tight-binding approximation to TDDFT (TDDFT-TB),⁵⁴ using also the results of the PBE ground state calculations. For the CD spectra, the calculation of the rotatory strengths only requires as input the ground-state molecular orbitals (MOs) and the solutions of the Casida's equations obtained exactly or within whichever approximation, as is actually also the case for the calculation of the oscillator strengths. Thus, within TDDFT-TB, the solutions of the approximated Casida's equations⁵⁴ and the ground-state MOs are used to compute the oscillator strengths⁵⁴ and also the rotatory strengths and the electric and magnetic transition dipole moments as described in Refs 52,53. A good agreement is observed between the TDDFT and TDDFT-TB results obtained for $[\text{Au}_{38}(\text{SCH}_3)_{24}]$ (see below). Consequently, using the PBE functional, the computationally less demanding TDDFT-TB method was employed for the characterization of the 1500 lowest-lying dipole-allowed electronic excitations of the $[\text{Au}_{38}(\text{SCH}_3)_{24}]$ and $[\text{Au}_{38}(\text{SCH}_3)_{23}(\text{TH4})]$ model clusters. Scalar-relativistic effects were included in the electronic excitation calculations, which were all performed with the ADF2019.107 release of the ADF program package.

Results and discussion

In general, the concept of ligand exchange reaction relies on tuning the chiroptical properties of the native cluster and introducing new functionalities by carefully choosing appropriate, functional ligands. Since the thiol TH4 ligand is intrinsically chiral, one could expect a change of the CD signals of Au_{38} cluster after ligand exchange reaction, in case of an enantiomeric selection of the ligand.



Scheme 2 Schematic representation of the ligand exchange reaction between Au_{38} cluster and TH4 ligand. The gold atoms on the staples are coloured in orange, sulphur atoms are in green. The leaving 2-PET ligand is highlighted in blue and the incoming TH4 in magenta.

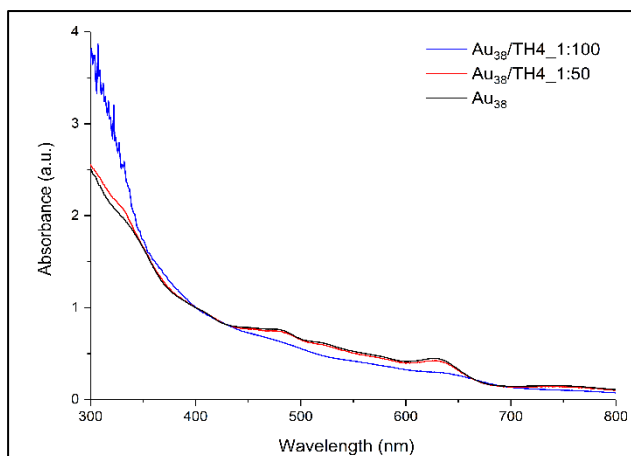


Fig. 1 UV-vis spectra of exchange samples using 1:50 and 1:100 cluster/ligand molar ratios. The UV-vis spectrum of $\text{Au}_{38}(\text{2-PET})_{24}$ is used as a reference. The spectra were measured in toluene and are normalized at 400 nm for comparison.

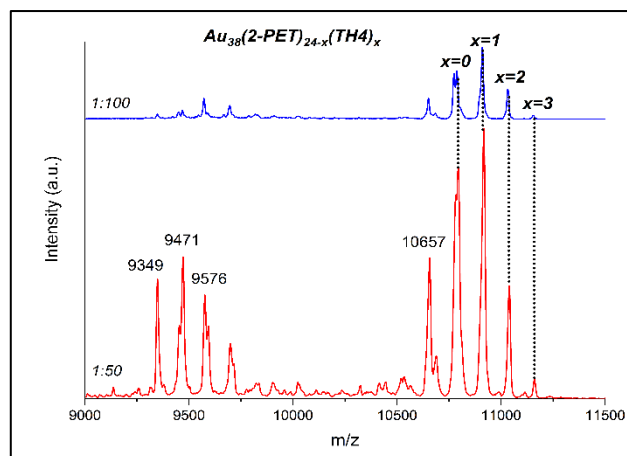


Fig. 2 MALDI analyses of the samples after ligand exchange reactions using 1:50 and 1:100 cluster/ligand molar ratios. The exchanged species are presented by the symbol "x".

However, as TH4 is configurationally labile, the ligand was always in the racemic form in solution in the ligand exchange process with both racemic and enantiopure cluster. The ligand exchange reaction between intrinsically chiral $\text{Au}_{38}(\text{2-PET})_{24}$ cluster (racemic mixture) and TH4 ligand was carried out at 50 °C by using different cluster/ligand molar ratios (1:20, 1:50 and 1:100). Note, that one incoming TH4 ligand exchanges with one 2-PET ligand leading to the formation of clusters with an $\text{Au}_{38}(\text{2-PET})_{24-x}(\text{TH4})_x$ composition as shown in Scheme 2.

First, two initial cluster/ligand ratios (1:50 and 1:100) were used to study the effect of the ligand concentration on the total number of exchange product on the cluster surface. Preliminary analyses (not shown) showed that high concentrations of helical ligand (above 10 equivalents of ligand) are necessary to drive the ligand exchange reaction forward and thus, two concentrations as mentioned above were used. The UV-vis spectrum of the $\text{Au}_{38}(\text{2-PET})_{24}$ before the reaction was recorded to be further used as a reference. According to the UV-vis results in Fig. 1, the spectrum of 1:50 cluster/ligand molar ratio perfectly matches with the reference. No obvious changes are evident on the absorption spectrum upon ligand exchange reaction between leaving 2-PET ligand and incoming TH4 ligand.

Yet, several exchanged species were formed in the solution according to the MALDI analysis (to be discussed later). However, with increasing the concentration of ligand (100 equivalents with respect to cluster), the characteristic absorption fingerprints of the cluster become less expressed at higher wavelengths. Additionally, at lower wavelengths, i.e. below 400 nm, a strong increase in absorbance is mostly ascribed to the TH4 ligand (Fig. S1A†).

According to MALDI analyses (Fig. 2), up to three TH4 ligands were successfully exchanged on the cluster surface. The mass difference between incoming and the leaving ligand is about m/z 123 thus giving rise to a mass spectrum with equally spaced ($\Delta m = 123$) peaks corresponding to the addition of TH4 ligands to the parent cluster. From the mass spectra the average exchange number can be calculated.

By doing so, $\bar{x}=0.87$ and $\bar{x}=0.93$ were calculated for 1:50 and 1:100 cluster/ligand molar ratios respectively (Table S1†). We noted that depending on the ionization (laser) power in the mass spectrometer, the relative intensities of most abundant species in the sample varied however, the maximal exchange number of TH4 ligand has not been much affected.

Besides our efforts to minimize fragmentation of the sample under applied ionization power, different fragments reached the detector and were carefully examined. As such, the mass difference between m/z 9458 and the parent peak at m/z 10778 is +1336 which corresponds to the very well-known cyclic $\text{Au}_4(\text{2-PET})_4$ fragment typical for all gold clusters.⁵⁵ It is believed that the tetrameric fragment unit is formed from the staple motifs⁵⁶ and thus provides a valuable information about the surface composition. It is especially very useful for the analysis of mixed ligand shell cluster.

Hence, the presence of this fragment with incorporated TH4 ligand such as $\text{Au}_4(\text{2-PET})_3\text{TH4}$, $\text{Au}_4(\text{2-PET})_2(\text{TH4})_2$, $\text{Au}_4(\text{2-PET})(\text{TH4})_3$ and $\text{Au}_4(\text{TH4})_4$ was highly anticipated in the mass spectrum. Careful inspection of the mass spectrum at very low m/z range (1200-1900) for the sample containing up to 3 exchanged species (1/100 cluster/ligand ratio, top panel in Fig. 2) shows the formation of $\text{Au}_4(\text{2-PET})_{4-x}(\text{TH4})_x$ substituted cyclic species with $x=0-2$ (Fig. S2†). Note that higher substituted fragments ($x=3,4$) were also detected for the samples containing more TH4 ligands on the surface (not shown).

Furthermore, up to nine TH4 ligands ($\bar{x}=4.3$) were exchanged with 2-PET ligand on Au_{38} cluster when leaving the reaction to proceed for longer times, on a large scale of starting reactants (Fig. S3†). In general, maximum ten TH4 ligands can be adsorbed on the cluster (to be discussed later). Further changes in the reaction conditions did not lead to further exchange. In particular it was not possible to prepare a cluster with 24 TH4 ligands. Possibly, the limitation in having more TH4 ligands contributing to the final composition of the mixed ligand shell can be explained considering the rigidity and bulkiness of the TH4 ligand. In fact, the more TH4 ligands adsorb on the cluster surface, the more sterically hindered the

neighbouring ligands become. This, on the other hand, vastly decreases the spatial distances between adjacent ligands and thus the repulsion between them becomes at some point unavoidable. As a matter of fact, the decomposition of the cluster due to the induced instability on the surface can take place. Indeed, we have noticed the formation of a thin plasmonic layer and insoluble by-products around the flask after ligand exchange reaction when bigger amount of TH4 ligand was introduced to the reaction mixture.

Moreover, the increase of the number of helical ligands on the cluster surface has a direct influence on its UV-vis spectrum. Precisely, the absorption bands between 400 to 600 nm flatten and the well-pronounced peak at around 630 nm is even slightly red shifted (with respect to the reference spectrum of Au_{38} , Fig. S4[†]). Previously, similar phenomenon has also been observed for the ligand exchange reaction with dithiol BINAS ligand.²⁸ Even though the characteristic optical fingerprints of the Au_{38} have been diminished, the core size of the cluster has been preserved during the ligand exchange process.

Next, since the optical properties of the cluster are strongly affected by attaching the helical ligand to the cluster, we anticipated changes in chiroptical properties of the cluster.

To test our hypothesis, first, the left-handed (E1) and right-handed (E2) enantiomers of the chiral $Au_{38}(2-PET)_{24}$ cluster were separated on HPLC according to the previously described protocol.⁵⁷ Afterwards, similar ligand exchange procedure as mentioned above has been carried out. The only difference is that the ligand exchange was performed at room temperature to avoid the racemization of the cluster.⁵⁸ Moreover, the initial concentration of the TH4 ligand was reduced to 20 equivalents in order to slow down the ligand exchange rate and have less exchanged TH4 on the cluster surface. Besides, we aimed to see the effect of a single helicene on optical and chiral properties of the cluster. To start with, the reaction products were first characterized by UV-vis spectroscopy and MALDI mass spectrometry. UV-vis analyses (Fig. S5[†]) do not show any changes on the optical fingerprints of the cluster (similar to what we have observed when using 50 equivalents of TH4

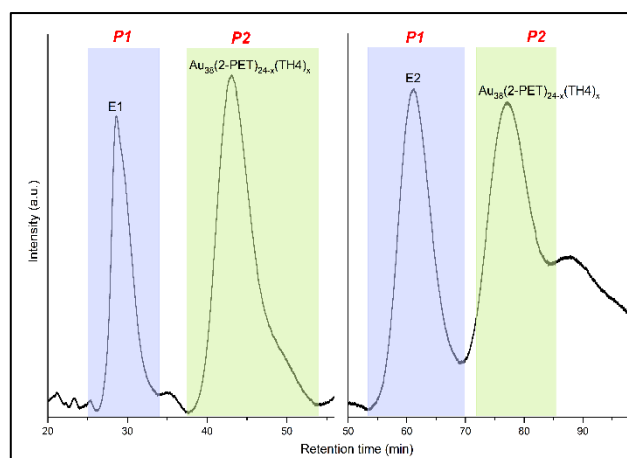


Fig. 3 HPLC chromatograms of E1/E2+TH4 (20 equivalents of TH4 ligand). The eluting peaks were detected at 300 nm. The peak of exchanged products is highlighted in green, whereas the parent cluster is marked in purple. E1 and E2 are left- and right-handed enantiomers of $Au_{38}(2-PET)_{24}$ cluster, respectively.

ligand) whereas MALDI showed the appearance of up to 3 exchange species in the mass spectra at higher m/z for both enantiomers of the cluster (Fig. S6[†]). The exchanged species $Au_{38}(2-PET)_{24-x}(TH4)_x$ (where x is up to 3) were separated from the unreacted parent Au_{38} cluster on HPLC system using the same separation protocol and conditions as reported for the enantioseparation of Au_{38} (Fig. 3).⁵⁷

After passing the crude mixture in SEC column to purify from free ligand, a small volume of the reaction mixture (20 μ L) was injected into the chiral HPLC column operating at normal isocratic elution mode.

In the chromatograms, the first peaks associated with enantiopure cluster were labelled as P1 (25-33 min and 54-70 min for E1 and E2 respectively) whereas the exchanged products of both enantiomers were named P2 (35-52 min and 72-85 min for exchanged species) (Fig. 3).

Note, P1 peaks of unreacted enantiomers (E1 and E2) have sharp and symmetric shapes and elute earlier (short retention times) whereas P2 peaks of exchanged species retain longer

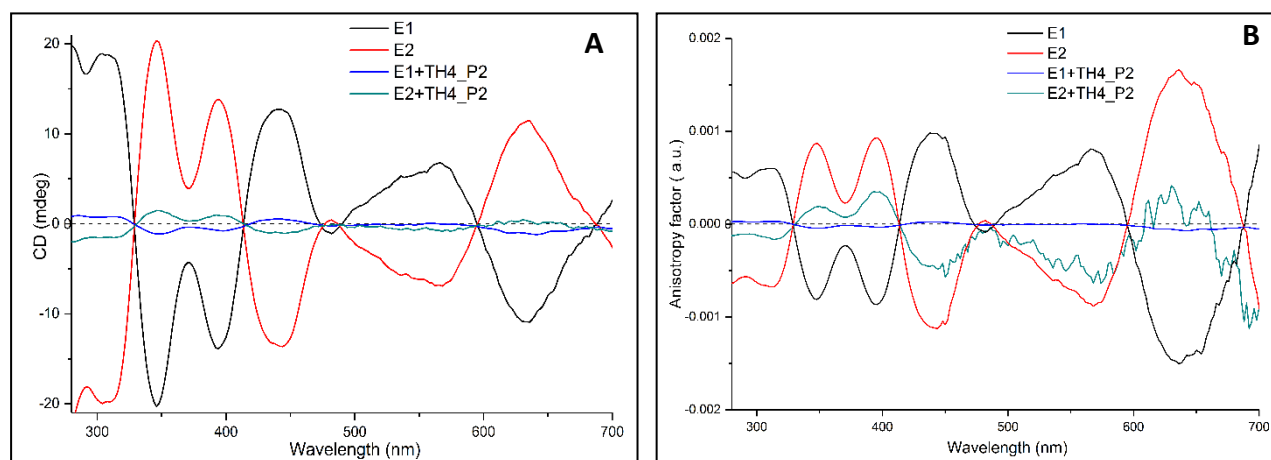


Fig. 4 (A) CD responses and (B) anisotropy factors g of samples and their references (E1 and E2 enantiomers of $Au_{38}(2-PET)_{24}$). Both the samples and the reference were measured in DCM and the solvent background was subtracted afterwards. 1:20 cluster/ligand molar ratios were used for the ligand exchange reaction.

inside the column and have more asymmetric shape with a larger peak width. This means that several exchange products are contributing to it and since they are not well resolved, they all come out as a single peak at higher retention times.

A small broad peak after P2 of the second enantiomer of cluster has also been observed; unfortunately, further analysis of this peak was not successful. Moreover, new peaks matching well with the HPLC retention profiles of pure enantiomers of the cluster also elute in the chromatogram. Note that, the peak of the opposite enantiomer was not present before the reaction (Fig. S7[†]). Since only enantiopure Au₃₈ was used for each ligand exchange reaction, the appearance of the other enantiomer in the chromatogram indicates the partial racemization of the cluster. It was previously shown,⁵⁸ that the racemization of enantiopure Au₃₈(2-PET)₂₄ cluster takes place at relatively high temperatures, i.e. 50 °C and above. Our result indicates that the adsorbed TH4 ligand accelerates the racemization of the cluster thus leading to appreciable racemization even at room temperature. However, we cannot draw a definitive conclusion about that since no systematic studies on racemization of the cluster after ligand exchange reaction have been performed. Recently, Malola *et al* proposed a mechanism for the racemization of Au₃₈ based on calculations which involves the reconstruction of the metallic core without breaking a Au-S bond.⁵⁹ In this case, it is possible that the adsorption of the TH4 ligand onto the cluster surface accelerates the rotation of the three Au atoms at the pole of the cluster resulting in the rearrangement of long staple motifs into the opposite enantiomer. Furthermore, we cannot exclude the possibility that the fact that the TH4 ligand was in the racemic mixture plays a role in racemization of the cluster. However, to draw definitive conclusions, one would need to study the effect of enantiopure TH4 on the racemization of the cluster, which, unfortunately, is not possible with TH4 ligand (as mentioned earlier in the introduction). Possibly, the influence of the ligand on the electronic structure of the cluster plays a role in this process.

If our hypothesis is correct, one would expect to see changes and variations in CD spectrum. For that, P2 peaks were collected repeatedly after each injection step and analysed by CD spectroscopy (Fig. 4A). The calculated CD spectrum of a non-functionalized *M*-[4]helicene has several negative and positive bands all positioned below 330 nm.³² Since the cluster itself has a strong absorption below 300 nm, the contribution of exchanged TH4 ligand to the chiral signals of the cluster are obscured. Nonetheless, the metal-based CD responses in the visible region of the spectrum are drastically decreased when comparing with the reference cluster. However, the intensity does not reach to zero value and both spectra are still mirror images to each other. The characteristic transitions at around 350, 400, 450, 570 and 630 nm are still recognizable. Since the intensity of CD signals is concentration dependent, to make the comparison more trustworthy, the concentration factor was excluded by calculating the anisotropy factor *g* for each enantiopure sample (Fig. 4B). The *g* factors of the exchange species of the first enantiomer (E1) are hugely affected and

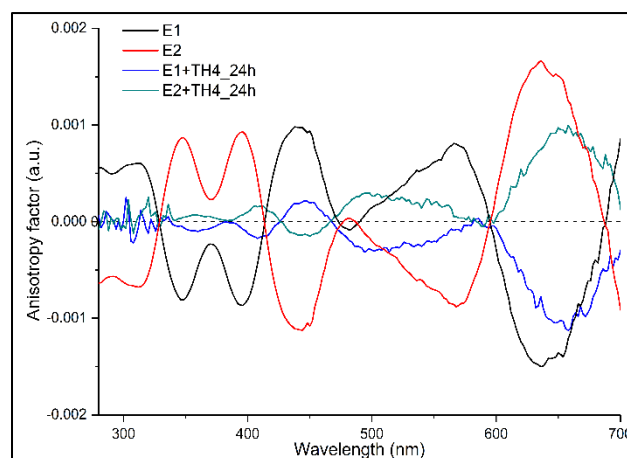


Fig. 5 Anisotropy factors *g* of exchanged samples and their references (E1 and E2 enantiomers of Au₃₈(2-PET)₂₄) measured in DCM. The solvent background has been subtracted afterwards. 1:100 cluster/ligand molar ratios were used for the ligand exchange reaction.

became very weak. As is shown in Fig. S6[†], the MALDI analyses show more exchanged species with higher intensities for the first enantiomer. Although the same reaction conditions were applied for the ligand exchange reactions with both enantiomers of the cluster, it is not surprising, in our experience, that different exchange rates are observed for different experiments, which explains the observed changes and variations in the intensity of the CD spectra and in the total exchange number (evidenced from MALDI in Fig. S6[†]), as well as the lack of mirror symmetry in *g* factor curves in Fig. 4B. This on the other hand indicates that, as one can anticipate, the influence on the electronic structure of the cluster increases with increasing number of helicene ligands in its ligand shell.

To further corroborate this, another ligand exchange reaction was carried out under modified reaction conditions. Specifically, a higher ligand to cluster ratio was used (100:1) and the reaction mixture was left to stir for 24 h at room temperature. As we have seen before, the UV-vis spectra for each enantiomeric sample showed less expressed features in the visible region (not shown). MALDI mass spectrum shows up to ten exchanged species (\bar{x} =3 and \bar{x} =2.4 for the first and the second enantiomers respectively) in both samples (Fig. S8[†]).

Table 1 Wavelengths and anisotropy factors *g* for enantiomer 2 (right-handed, E2) and corresponding exchange sample. 1:100 cluster/ligand molar ratios were used for the ligand exchange reaction.

Enantiomer 2 (E2)		E2+TH4	
Wavelength (nm)	<i>g</i> factor (a.u.)	Wavelength (nm)	<i>g</i> factor (a.u.)
348	8.6×10^{-4}	359	6.51×10^{-5}
395	9.12×10^{-4}	408	1.64×10^{-4}
444	-1.1×10^{-3}	445	-1.4×10^{-4}
568	-8.7×10^{-4}	495	2.86×10^{-4}
636	1.6×10^{-3}	655	9.48×10^{-4}

When comparing the anisotropy factors g of the exchanged products with the reference enantiopure cluster, not only the intensity of the peaks drops down (for some peaks drastically), but surprisingly almost all the peaks red shift (Fig. 5 and Table 1). Besides, the peak at around 570 nm for the E2 enantiomer of the cluster, which is blue shifted by about 73 nm after ligand exchange, even switched its sign with respect to the parent cluster. To further corroborate our findings and pinpoint the effect of the helical ligand on the chiroptical properties of the cluster, we have performed another set of ligand exchange reactions using racemic and enantiopure TH6-Br ligand (Fig. S1B-D[†]). Unlike TH4, TH6-Br is quite rigid, has significantly high racemization barrier (*ca.* 157 kJ/mol)³⁴ and thus can be obtained in enantiopure form.

The following ligand exchange reactions were performed at room temperature with 1:20 cluster/ligand ratios: (i) enantiopure Au₃₈(2-PET)₂₄ with racemic TH6-Br (noted as E1/E2+*rac*TH6-Br) and (ii) racemic Au₃₈(2-PET)₂₄ with enantiopure TH6-Br (noted as *rac*Au₃₈(2-PET)₂₄+*M*-TH6-Br). Note, in the latter case only *M*-TH6-Br was studied (due to the availability of *M*-form of the ligand). As evidenced from the UV-vis spectra of E1/E2+*rac*TH6-Br (Fig. S9[†]), after 20 h of reaction, a slight increase in absorbance at *ca.* 350 nm was observed mostly ascribable to the helical ligand. MALDI showed on average \bar{x} =0.23 and \bar{x} =0.1 exchanged TH6-Br ligand on the surface of E1 and E2 enantiomers, respectively (Fig. S10[†]). On the same note, slight differences were observed in CD spectra and corresponding anisotropy factors g after the attachment of helicenes (Fig. S11[†]). When similar ligand exchange reaction of racemic cluster and enantiopure ligand was followed *in situ* by HPLC technique, here, enantiospecific recognition behaviour was clearly observed especially in the early stages of the exchange process (Fig. S12A[†]). In brief, after the addition of *M*-TH6-Br, the intensity of E1 enantiomer drops down by 30 % and additional peaks (P1 and P2) appear at slightly higher retention times. At the same time, the intensity of E2 drops down by 14 %. P3 peak appears after 7.5 h of reaction. The plot of peaks' area vs retention times clearly shows that the ligand exchange is much faster and preferable for E1 at earlier reaction times (5 h, Fig. S12B[†]) and that one of the products has actually the same retention time as the parent cluster. More interestingly, the areas for P1 and P3 increase very slowly and have similar kinetic profiles, whereas P2 increases much faster and probably contains exchange species of both E1 and E2 enantiomers (based on the changes of enantiomers areas). It is possible that P1 and P3 correspond to one exchange and P2 to higher exchange species or they correspond to different exchange positions on the cluster. Furthermore, the UV-vis spectra after the HPLC monitoring (before passing through the SEC column to get rid of free ligand and after SEC) shows the diminishing of the cluster's native optical fingerprints at higher wavelengths (Fig. S13A[†]). On the contrary, at lower wavelengths (around 350 nm) an additional peak appears which originates from the adsorbed ligand. Moreover, MALDI mass spectrometry shows the formation of up to two exchange species with an average exchange number (\bar{x}) of 0.66 (Fig.

S13B[†]). Based on the HPLC peaks' areas 41 % of the cluster contains exchange species (both different numbers and positions for the same ligand, see details in the Supporting Information). In virtue of the above-mentioned additional results, we can undoubtedly confirm the paramount role of the rigidity of the helical ligand on the chiroptical properties of Au₃₈ cluster. On the other hand, these results brace the significant differences in two ligands and subsequent results obtained earlier.

Previously O. Lopez-Acevedo *et al* have studied the electronic and optical properties of Au₃₈ cluster by DFT computations.¹² The computational model satisfactorily reproduced the experimental CD spectrum and made the assignments of peaks at low energy possible. As such it has been shown that the peaks between 0.9-1.4 eV (1377-886 nm) arise from the combination of several metal-based HOMO-LUMO transitions. The high energy transitions at 1.6-2.2 eV (775-564 nm) include contributions from the ligand shell. Possibly the changes of the intensity and the sign especially for the peak at 568 nm is due to the TH4 ligand which influences the excitations out of the lower energy ligand orbitals.

Thus, based on the results we have presented so far, we can conclude that the ligand exchange reaction between 2-PET and TH4 ligands leads to the partial racemization of the enantiopure cluster as well as causes some changes in the electronic structure of the cluster. Going back to the question we addressed in the beginning, no preference for one enantiomer of the adsorbed TH4 helicene on the chiral cluster could be evidenced. However, we have conducted additional DFT calculations with the objective to probe the extent to which the optical properties of the cluster evolve upon the substitution of one ligand and to explore whether these changes depend on where the ligand exchange reactions take place at the cluster surface. Based on the crystal structure, Au₃₈ cluster consists of four symmetry unique sites: three on the long staples and one on the short staple at the waist. Thus, for a mono-exchanged species there are only four possible isomers (regioisomers). However, the number of possible regioisomers increases with increasing the number of exchanged ligands (e.g. 46 possible isomers upon the attachment of the second ligand). Considering the huge number of possible isomers upon the attachment of the TH4 ligand, to make the calculations doable, only a mono-exchanged species was considered for the further calculations.

DFT calculations

Results of the geometry optimization

We have considered the model cluster [Au₃₈(SCH₃)₂₄] (left-handed enantiomer, E1) and the one obtained by substituting a -SCH₃ ligand with the (*P*)-2-thio[4]helicene (TH4). For the substituted [Au₃₈(SCH₃)₂₃(TH4)] clusters, three regioisomers have been considered (see below).

Fig. 6 shows the optimized gas-phase structure of [Au₃₈(SCH₃)₂₄] and those of the three representative regioisomers of [Au₃₈(SCH₃)₂₃(TH4)] retained for the study.

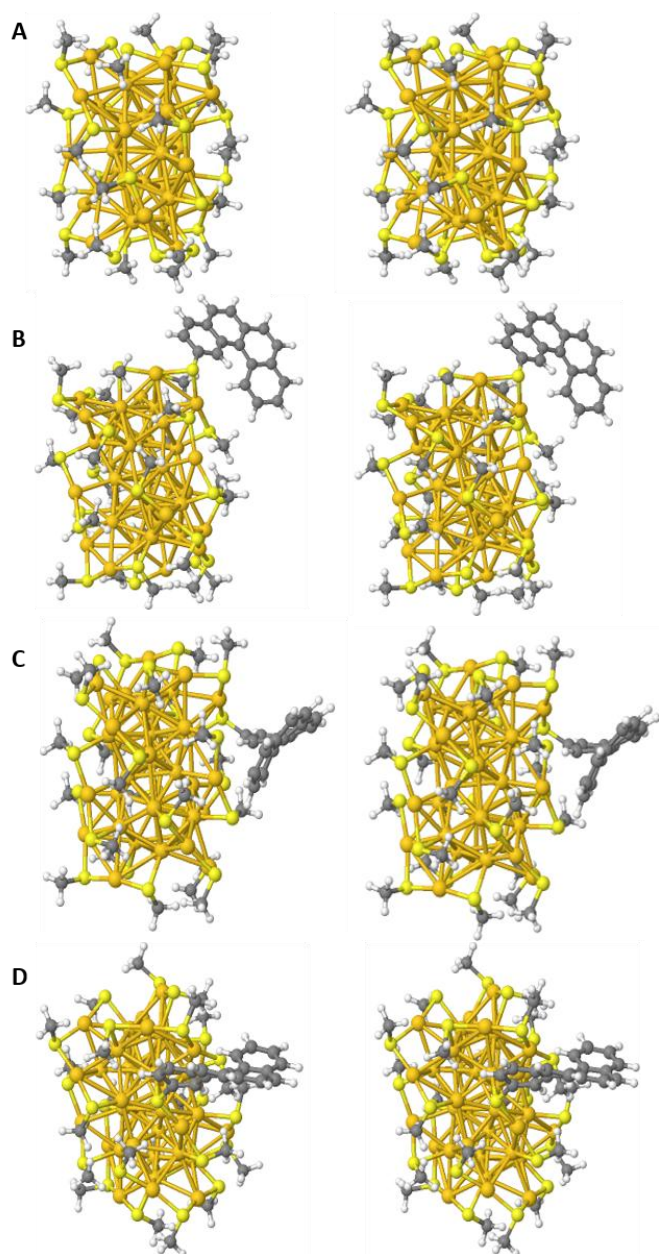


Fig. 6 (A) Stereoscopic view of the optimized geometry of $[\text{Au}_{38}(\text{SCH}_3)_{24}]$. (B) Stereoscopic view of the optimized geometry of the regioisomer A of $[\text{Au}_{38}(\text{SCH}_3)_{23}(\text{TH}_4)]$, denoted $[\text{Au}_{38}(\text{SCH}_3)_{23}(\text{TH}_4)]_{\text{A}}$. (C) Stereoscopic view of the optimized geometry of the regioisomer B of $[\text{Au}_{38}(\text{SCH}_3)_{23}(\text{TH}_4)]$, denoted $[\text{Au}_{38}(\text{SCH}_3)_{23}(\text{TH}_4)]_{\text{B}}$. (D) Stereoscopic view of the optimized geometry of the regioisomer C of $[\text{Au}_{38}(\text{SCH}_3)_{23}(\text{TH}_4)]$, denoted $[\text{Au}_{38}(\text{SCH}_3)_{23}(\text{TH}_4)]_{\text{C}}$.

The atomic coordinates are available as Supplementary Information (XYZ format).

The comparison of the electronic energies of the regioisomers shows that the regioisomer A is the most stable, B and C lying higher in energy by only 492 cm^{-1} and 449 cm^{-1} , respectively.

Chiroptical properties

$[\text{Au}_{38}(\text{SCH}_3)_{24}]$: assessment of the performance of the TDDFT-TB method

Using the TDDFT and TDDFT-TB results for the 300 lowest-lying dipole-allowed transitions of $[\text{Au}_{38}(\text{SCH}_3)_{24}]$, its absorption and

CD spectra have been simulated by convoluting the calculated oscillator and rotatory strengths with Gaussians having a full width at half maximum (FWHM) of 2000 cm^{-1} . They are plotted along with the deduced anisotropy factor in Fig. S14[†] and Fig. S15[†] as function of the transition energy and wavelength, respectively. A good agreement is observed between the spectra obtained using the TDDFT and TDDFT-TB results.

Using the TDDFT-TB results for the 1500 lowest-lying dipole-allowed transitions, the absorption and CD spectra of $[\text{Au}_{38}(\text{SCH}_3)_{24}]$ have also been simulated. They are plotted along with the associated anisotropy factor in Fig. S16[†] and Fig. S17[†] as function of the transition energy and wavelength, respectively. A good agreement is observed between the curves predicted from the TDDFT-TB results and the experimental ones (Fig. S18[†]).⁵⁷ This agreement and the one previously observed between the spectra obtained using the TDDFT and TDDFT-TB results validate the use of the TDDFT-TB method for characterizing the chiroptical properties of the Au_{38} clusters over an energy range as large as the one shown in Fig. S16[†].

Comparison of the chiroptical properties of the $[\text{Au}_{38}(\text{SCH}_3)_{24}]$ and $[\text{Au}_{38}(\text{SCH}_3)_{24}(\text{TH}_4)]$ clusters

The simulated absorption and CD spectra of $[\text{Au}_{38}(\text{SCH}_3)_{24}]$ and the regioisomers of $[\text{Au}_{38}(\text{SCH}_3)_{23}(\text{TH}_4)]$ are plotted in Fig. S19[†] and Fig. 7 as function of the transition energy and wavelength, respectively. Noticeable changes in the absorption and CD spectra are observed upon ligand exchange. These changes depend on the site where the exchange took place. These changes are emphasized by the plots in Fig. S20[†] and Fig. S21[†] of the differences between the simulated absorption and CD spectra of the $[\text{Au}_{38}(\text{SCH}_3)_{23}(\text{TH}_4)]$ clusters and those of the $[\text{Au}_{38}(\text{SCH}_3)_{24}]$ cluster taken as references.

Charge-transfer transitions between the Au_{38} cluster and the TH4 ligand

Charge transfer (CT) transitions are expected to occur between the Au_{38} cluster and the TH4 ligand and to involve the π orbitals of the latter. This can be seen by inspecting the transitions between natural transition orbitals (NTOs).⁶⁰

To ease and make efficient the identification of such CT transitions in the three isomers, the TDDFT-TB calculations have been performed again using as basis set the molecular orbitals of the $[\text{Au}_{38}(\text{SCH}_3)_{23}]^+$ and TH_4^- fragments, and computing for their 1500 transitions the statistical descriptors proposed by Plasser and Lischka.⁶¹ The descriptor of interest to us here is the charge transfer character (CT) which varies between 0 (for locally excited or Frenkel excitonic states) and 1 (for completely charge separated states). For the three isomers, the calculated CT is in the range $0.0\sim 0.5$; the features of their five transitions having the highest CT are summarized in Tables S2[†]–S4[†]. A LibreOffice spreadsheet summarizing for each isomer the features of the characterized 1500 electronic transitions, i.e. their energies and wavelengths, their oscillator and rotatory strengths, and selected statistical descriptors, is provided in the supplementary materials.

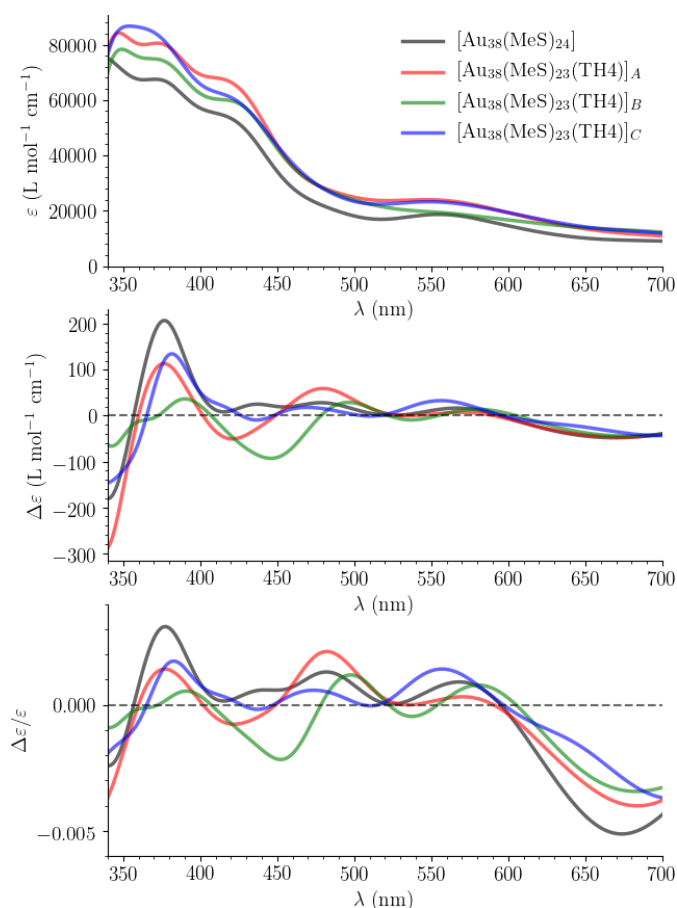


Fig. 7 Simulated absorption and CD spectra of the $[\text{Au}_{38}(\text{SCH}_3)_{24}]$ and $[\text{Au}_{38}(\text{SCH}_3)_{23}(\text{TH}_4)]$ clusters obtained by convoluting the calculated oscillator and rotatory strengths with Gaussians having a FWHM of 2000 cm^{-1} : they are plotted along with the anisotropy factor as functions of the transition wavelength (TDDFT-TB results for the 1500 lowest-lying dipole-allowed transitions).

Conclusions

We have shown that the ligand exchange reaction between intrinsically chiral $\text{Au}_{38}(\text{2-PET})_{24}$ and TH4 ligand resulted in the formation of up to ten exchanged species with a composition of $\text{Au}_{38}(\text{2-PET})_{24-x}(\text{TH}_4)_x$. The adsorption of the helical ligand resulted in obvious changes on the optical spectrum of the cluster. The diminishing of the UV-vis bands intensity and even the red shift of some electronic transitions at higher ligand concentrations indicate changes in electronic structure upon ligand exchange reaction although the core size of the cluster has been preserved. HPLC monitoring of the reaction and separation of the enantiopure exchange products from their native cluster showed the appearance of the other enantiomer of the cluster in the solution. Thus, the ligand exchange reaction leads to the partial racemization of the cluster. On the other hand, the adsorption of the TH4 ligand significantly changes the CD line shapes and even causes the inversion of the sign of some peaks. With the exploratory computational study, we have shown (i) that the substitution of an achiral CH_3S -ligand in the $[\text{Au}_{38}(\text{SCH}_3)_{24}]$ model cluster by the chiral 2-thio[4]helicene ligand translates into noticeable changes in the absorption and CD spectra of the Au_{38} cluster, and that these

changes depend on the site where the substitution took place. (ii) We have also shown that there are charge transfer transitions between the Au_{38} cluster and the helicene ligand.

Conflicts of interest

There are no conflicts to declare.

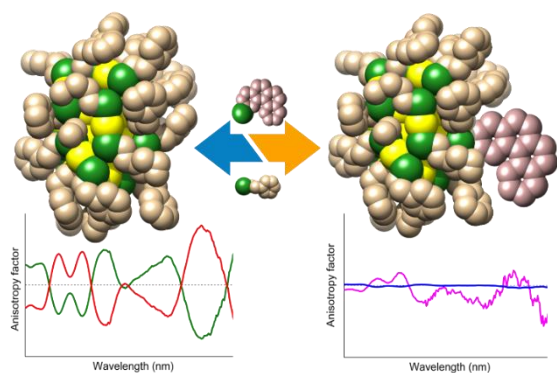
Acknowledgements

Financial support from Swiss National Science Foundation (Grant 200020_172511) and the University of Geneva is kindly acknowledged. Financial support in France by the CNRS, the University of Angers, the Région Pays de la Loire through the RFI LUMOMAT (grants to K.M. and M.M.T.), the National Agency for Research (ANR, Project 15-CE29-0006-01 ChiraMolCo) and the French Ministry of Foreign Affairs through the Germaine de Staël (PHC Project 39483PL) project is gratefully acknowledged. LDLM acknowledges a grant from the Swiss National Supercomputing Centre (CSCS) under project ID s894.

References

- 1 R. Jin, C. Zeng, M. Zhou and Y. Chen, *Chem. Rev.*, 2016, **116**, 10346–10413.
- 2 I. Chakraborty and T. Pradeep, *Chem. Rev.*, 2017, **117**, 8208–8271.
- 3 O. Varnavski, G. Ramakrishna, J. Kim, D. Lee and T. Goodson, *J. Am. Chem. Soc.*, 2010, **132**, 16–17.
- 4 M. C. M. Daniel and D. Astruc, *Chem. Rev.*, 2004, **104**, 293–346.
- 5 N. L. Rosi, D. A. Giljohann, C. S. Thaxton, A. K. R. Lytton-Jean, M. S. Han and C. A. Mirkin, *Science (80-.)*, 2006, **312**, 1027–1030.
- 6 N. T. Kim Thanh and Z. Rosenzweig, *Anal. Chem.*, 2002, **74**, 1624–1628.
- 7 C. M. Niemeyer, *Angew. Chemie Int. Ed.*, 2001, **40**, 4128–4158.
- 8 H. Wohltjen and A. W. Snow, *Anal. Chem.*, 1998, **70**, 2856–2859.
- 9 N. Zheng and G. D. Stucky, *J. Am. Chem. Soc.*, 2006, **128**, 14278–14280.
- 10 M. Pumera, J. Wang, E. Grushka and R. Polsky, *Anal. Chem.*, 2001, **73**, 5625–5628.
- 11 R. Jin, *Nanoscale*, 2015, **7**, 1549–1565.
- 12 O. Lopez-Acevedo, H. Tsunoyama, T. Tsukuda, H. Häkkinen and C. M. Aikens, *J. Am. Chem. Soc.*, 2010, **132**, 8210–8218.
- 13 I. Dolamic, B. Varnholt and T. Bürgi, *Nat. Commun.*, 2015, **6**, 7117.
- 14 B. Nieto-Ortega and T. Bürgi, *Acc. Chem. Res.*, 2018, **51**, 2811–2819.
- 15 S. Knoppe and T. Bürgi, *Acc. Chem. Res.*, 2014, **47**, 1318–1326.
- 16 R. Philip, P. Chantharasupawong, H. Qian, R. Jin and J.

- Thomas, *Nano Lett.*, 2012, **12**, 4661–4667.
- 17 H. Inouye, K. Tanaka, I. Tanahashi and K. Hirao, *Phys. Rev. B*, 1998, **57**, 11334–11340.
- 18 M. Cui, Y. Zhao and Q. Song, *TrAC Trends Anal. Chem.*, 2014, **57**, 73–82.
- 19 X. Qu, Y. Li, L. Li, Y. Wang, J. Liang and J. Liang, *J. Nanomater.*, 2015, **2015**, 1–23.
- 20 H. Häkkinen, M. Walter and H. Grönbeck, *J. Phys. Chem. B*, 2006, **110**, 9927–9931.
- 21 H. Qian, Y. Zhu and R. Jin, *ACS Nano*, 2009, **3**, 3795–3803.
- 22 H. Qian, W. T. Eckenhoff, Y. Zhu, T. Pintauer and R. Jin, *J. Am. Chem. Soc.*, 2010, **132**, 8280–8281.
- 23 Y. Niihori, S. Hossain, B. Kumar, L. V. Nair, W. Kurashige and Y. Negishi, *APL Mater.*, DOI:10.1063/1.4978373.
- 24 C. Zeng, C. Liu, Y. Pei and R. Jin, *ACS Nano*, 2013, **7**, 6138–6145.
- 25 A. Das, C. Liu, C. Zeng, G. Li, T. Li, N. L. Rosi and R. Jin, *J. Phys. Chem. A*, 2014, **118**, 8264–8269.
- 26 S. Knoppe, R. Azoulay, A. Dass and T. Bürgi, *J. Am. Chem. Soc.*, 2012, **134**, 20302–20305.
- 27 L. Beqa, D. Deschamps, S. Perrio, A. C. Gaumont, S. Knoppe and T. Bürgi, *J. Phys. Chem. C*, 2013, **117**, 21619–21625.
- 28 S. Knoppe, A. C. Dharmaratne, E. Schreiner, A. Dass and T. Bürgi, *J. Am. Chem. Soc.*, 2010, **132**, 16783–16789.
- 29 Y. Wang, B. Nieto-Ortega and T. Bürgi, *Chem. Commun.*, 2019, **55**, 14914–14917.
- 30 C. Zeng, H. Qian, T. Li, G. Li, N. L. Rosi, B. Yoon, R. N. Barnett, R. L. Whetten, U. Landman and R. Jin, *Angew. Chemie Int. Ed.*, 2012, **51**, 13114–13118.
- 31 Y. Shen and C. F. Chen, *Chem. Rev.*, 2012, **112**, 1463–1535.
- 32 F. Furche, R. Ahlrichs, C. Wachsmann, E. Weber, A. Sobanski, F. Vögtle and S. Grimme, *J. Am. Chem. Soc.*, 2000, **122**, 1717–1724.
- 33 S. Grimme and S. D. Peyerimhoff, *Chem. Phys.*, 1996, **204**, 411–417.
- 34 J. Barroso, J. L. Cabellos, S. Pan, F. Murillo, X. Zarate, M. A. Fernandez-Herrera and G. Merino, *Chem. Commun.*, 2017, **54**, 188–191.
- 35 C. Wäckerlin, J. Li, A. Mairena, K. Martin, N. Avarvari and K. H. Ernst, *Chem. Commun.*, 2016, **52**, 12694–12697.
- 36 S. Knoppe, J. Boudon, I. Dolamic, A. Dass and T. Bürgi, *Anal. Chem.*, 2011, **83**, 5056–5061.
- 37 R. H. Martin, J. Moriau and N. Defay, *Tetrahedron*, 1974, **30**, 179–185.
- 38 M. A. Brooks and L. T. Scott, *J. Am. Chem. Soc.*, 1999, **121**, 5444–5449.
- 39 T. Biet, A. Fihey, T. Cauchy, N. Vanthuyne, C. Roussel, J. Crassous and N. Avarvari, *Chem. - A Eur. J.*, 2013, **19**, 13160–13167.
- 40 P. Hohenberg and W. Kohn, *Phys. Rev.*, 1964, **136**, B864–B871.
- 41 W. Kohn and L. J. Sham, *Phys. Rev.*, 1965, **140**, A1133–A1138.
- 42 G. te Velde, F. M. Bickelhaupt, E. J. Baerends, C. Fonseca Guerra, S. J. A. van Gisbergen, J. G. Snijders and T. Ziegler, *J. Comput. Chem.*, 2001, **22**, 931–967.
- 43 C. Fonseca Guerra, J. G. Snijders, G. Velde and E. J. Baerends, *Theor. Chem. Acc.*, 1998, **99**, 391–403.
- 44 ADF; SCM, Theoretical Chemistry; Vrije Universiteit: Amsterdam, The Netherlands. <https://www.scm.com>.
- E. J. Baerends, T. Ziegler, A. J. Atkins, J. Autschbach, D. Bashford, O. Baseggio, A. Bérces, F. M. Bickelhaupt, C. Bo, P. M. Boerritger, L. Cavallo, C. Daul, D. P. Chong, D. V. Chulhai, L. Deng, R. M. Dickson, J. M. Dieterich, D. E. Ellis, M. van Faassen, A. Ghysels, A. Giammona, S. J. A. van Gisbergen, A. Goetz, A. W. Götz, S. Gusarov, F. E. Harris, P. van den Hoek, Z. Hu, C. R. Jacob, H. Jacobsen, L. Jensen, L. Joubert, J. W. Kaminski, G. van Kessel, C. König, F. Kootstra, A. Kovalenko, M. Krykunov, E. van Lenthe, D. A. McCormack, A. Michalak, M. Mitoraj, S. M. Morton, J. Neugebauer, V. P. Nicu, L. Noodleman, V. P. Osinga, S. Patchkovskii, M. Pavanello, C. A. Peebles, P. H. T. Philipsen, D. Post, C. C. Pye, H. Ramanantoanina, P. Ramos, W. Ravenek, J. I. Rodríguez, P. Ros, R. Rüger, P. R. T. Schipper, D. Schlüns, H. van Schoot, G. Schreckenbach, J. S. Seldenthuis, M. Seth, J. G. Snijders, M. Solà, S. M., M. Swart, D. Swerhone, G. te Velde, V. Tognetti, P. Vernooijs, L. Versluis, L. Visscher, O. Visser, F. Wang, T. A. Wesolowski, E. M. van Wezenbeek, G. Wiesenekker, S. K. Wolff, T. K. Woo and A. L. Yakovlev, .
- 45 J. P. Perdew, K. Burke and M. Ernzerhof, *Phys. Rev. Lett.*, 1996, **77**, 3865–3868.
- 46 S. Grimme, J. Antony, S. Ehrlich and H. Krieg, *J. Chem. Phys.*, 2010, **132**, 154104.
- 47 E. Van Lenthe and E. J. Baerends, *J. Comput. Chem.*, 2003, **24**, 1142–1156.
- 48 E. van Lenthe, A. Ehlers and E.-J. Baerends, *J. Chem. Phys.*, 1999, **110**, 8943–8953.
- 49 E. van Lenthe, E. J. Baerends and J. G. Snijders, *J. Chem. Phys.*, 1994, **101**, 9783–9792.
- 50 M. E. CASIDA, 1995, pp. 155–192.
- 51 S. J. A. van Gisbergen, F. Kootstra, P. R. T. Schipper, O. V. Gritsenko, J. G. Snijders and E. J. Baerends, *Phys. Rev. A*, 1998, **57**, 2556–2571.
- 52 J. Autschbach and T. Ziegler, *J. Chem. Phys.*, 2002, **116**, 891–896.
- 53 J. Autschbach, T. Ziegler, S. J. A. Van Gisbergen and E. J. Baerends, *J. Chem. Phys.*, 2002, **116**, 6930–6940.
- 54 R. Rüger, E. van Lenthe, T. Heine and L. Visscher, *J. Chem. Phys.*, 2016, **144**, 184103.
- 55 A. Dass, A. Stevenson, G. R. Dubay, J. B. Tracy and R. W. Murray, *J. Am. Chem. Soc.*, 2008, **130**, 5940–5946.
- 56 Y. Zhang, S. Shuang, C. Dong, C. K. Lo, M. C. Paau and M. M. F. Choi, *Anal. Chem.*, 2009, **81**, 1676–1685.
- 57 I. Dolamic, S. Knoppe, A. Dass and T. Bürgi, *Nat. Commun.*, 2012, **3**, 798.
- 58 S. Knoppe, I. Dolamic and T. Bürgi, *J. Am. Chem. Soc.*, 2012, **134**, 13114–13120.
- 59 S. Malola and H. Häkkinen, *J. Am. Chem. Soc.*, 2019, **141**, 6006–6012.
- 60 R. L. Martin, *J. Chem. Phys.*, 2003, **118**, 4775–4777.
- 61 F. Plasser and H. Lischka, *J. Chem. Theory Comput.*, 2012, **8**, 2777–2789.



TOC graphic: The ligand exchange reaction of intrinsically chiral Au₃₈ and helical TH4 ligand: the effect of the ligand on CD properties.